

Interactions of the Type III Secretion Pathway Proteins LcrV and LcrG from *Yersinia pestis* Are Mediated by Coiled-Coil Domains*

Received for publication, April 15, 2002, and in revised form, June 26, 2002
Published, JBC Papers in Press, July 9, 2002, DOI 10.1074/jbc.M203632200

Daniel G. Lawton[‡], Colin Longstaff[§], B. A. Wallace[¶], Jim Hill^{||}, Sophie E. C. Leary^{||},
Richard W. Titball^{||}, and Katherine A. Brown^{‡**}

From the [‡]Department of Biological Sciences, Centre for Molecular Microbiology and Infection, Flowers Building, Imperial College of Science, Technology and Medicine, London SW7 2AY, United Kingdom, the [§]Department of Haematology, National Institute for Biological Standards and Control, Blanche Lane, South Mimms, Potters Bar, Hertfordshire EN6 3QG, United Kingdom, the [¶]School of Crystallography, Birkbeck College, University of London, London WC1E 7HX, United Kingdom, and ^{||}Defense Science and Technology Laboratory, Chemical and Biological Sciences, Porton Down, Wiltshire SP4 0JQ, United Kingdom

The type III secretion system is used by pathogenic *Yersinia* to translocate virulence factors into the host cell. A key component is the multifunctional LcrV protein, which is present on the bacterial surface prior to host cell contact and up-regulates translocation by blocking the repressive action of the LcrG protein on the cytosolic side of the secretion apparatus. The functions of LcrV are proposed to involve self-interactions (multimerization) and interactions with other proteins including LcrG. Coiled-coil motifs predicted to be present are thought to play a role in mediating these protein-protein interactions. We have purified recombinant LcrV, LcrG, and site-directed mutants of LcrV and demonstrated the structural integrity of these proteins using circular dichroism spectroscopy. We show that LcrV interacts both with itself and with LcrG and have obtained micromolar and nanomolar affinities for these interactions, respectively. The effects of LcrV mutations upon LcrG binding suggest that coiled-coil interactions indeed play a significant role in complex formation. In addition, comparisons of secretion patterns of effector proteins in *Yersinia*, arising from wild type and mutants of LcrV, support the proposed role of LcrG in titration of LcrV *in vivo* but also suggest that other factors may be involved.

A number of Gram-negative bacteria use a conserved type III secretion system to transport a range of virulence-associated proteins across their double membranes and into the host cell (1). This mechanism plays a key role in the infection process of bacterial pathogens including *Chlamydia* sp., enteropathogenic and enterohemorrhagic *Escherichia coli*, *Pseudomonas aeruginosa*, *Shigella* sp., and *Yersinia* sp. (2). This system is a *sec*-independent pathway and is composed of approximately 20 proteins, a number of which are transiently assembled to form a “molecular syringe” that often results from a signal released upon contact with the target cell (2). This syringe structure is responsible for the translocation of protein “effectors” that can cause a range of

signaling and cytoskeletal changes upon the target cell, ultimately leading to, for example, intracellular invasion of a macrophage or apoptosis (3, 4).

The type III secretion system of *Yersinia* was the first to be discovered and is the best characterized to date. Therefore, it is considered to be the prototypical type III system. The genes encoding these proteins are located on plasmid pYV, which is present in all three human pathogenic *Yersinia* species, *i.e.* *Yersinia pseudotuberculosis*, *Yersinia enterocolitica*, and *Yersinia pestis*. These *Yersinia* species resist the primary host immune defense by inhibiting macrophage phagocytosis (2). This inhibition is mediated by the type III secretion system and thus allows infection by extracellular localization (5). The secretion machinery is principally composed of the *Yersinia* outer proteins (Yops),¹ the *Yersinia* secretion apparatus (Ysc), and specific Yop chaperones (Syc) (6).

A key component of the *Yersinia* type III secretion apparatus is the V antigen or LcrV, a 37-kDa protein, the expression of which is transcriptionally up-regulated at 37 °C upon infection of the host or *in vitro* in the absence of calcium (7). It is a protective antigen of *Y. pestis* (8, 9) and is currently in phase II trials as a principal component of a potential vaccine for plague (caused by *Y. pestis*) (1). LcrV has several putative roles in *Yersinia* type III secretion and *Yersinia* pathogenicity in general that are probably mediated by self-interactions (multimerization) or interactions with other proteins. LcrV has been proposed to assemble into a membrane-associated extracellular structure, which facilitates the transfer of Yop effector proteins into the eukaryotic cytosol, and is surface-located prior to target cell contact (10). Thus, the extracellular localization of LcrV on the bacterial membrane may provide a prime position from which to control Yop targeting (10). LcrV further promotes protein secretion and targeting through an interaction with YopB and YopD, possibly enabling their deployment for pore formation within the eukaryotic membrane (11). In addition, it has recently been demonstrated that LcrV is both extracellularly localized and translocated into the host cell cytosol (12).

LcrV has been predicted to contain a coiled-coil motif (13) composed of a repeating 7-residue signature sequence, indicative of the formation of a superhelix from two or more α -helices (reviewed in Refs. 14 and 15). Coiled-coils have been suggested

* This work was supported by the UK Biotechnology and Biological Sciences Research Council, UK Ministry of Defense, and Defense Science and Technology Laboratory. The costs of publication of this article were defrayed in part by the payment of page charges. This article must therefore be hereby marked “advertisement” in accordance with 18 U.S.C. Section 1734 solely to indicate this fact.

** To whom correspondence should be addressed. Tel.: 44-20-75945298; Fax: 44-20-75945207; E-mail: k.brown@ic.ac.uk.

¹ The abbreviations used are: Yop, *Yersinia* outer protein; Ysc, Yop secretion; ELISA, enzyme-linked immunosorbent assay; GST, glutathione S-transferase; PBS, phosphate-buffered saline; PBST, phosphate-buffered saline with Tween 20; CD, circular dichroism; SPR, surface plasmon resonance; MALDI-MS, matrix-assisted laser desorption ionization mass spectrometry.

to represent a key structural feature required for the formation of the multiprotein complexes involved with the type III secretion apparatus (13), and it has been suggested that the interaction of LcrV with the LcrG protein may be mediated through the formation of a coiled-coil (13). Genetic approaches such as the yeast-two hybrid system have been used to identify strong interactions between type III pathway proteins such as that observed between the EspA (filament-forming protein) and EspD (translocation pore proteins) of enteropathogenic *E. coli* (16). In *Yersinia*, similar experiments have demonstrated an interaction between LcrV and an inhibitory gate protein to the Ysc apparatus, LcrG (17). Overexpression of LcrG inhibits Yop secretion even in the presence of LcrV (18). Hence a "titration model" has been proposed whereby the up-regulation of LcrV during the low calcium response allows binding to LcrG, thus removing the internal gating of the Ysc apparatus (18). A site-directed mutant of LcrG was also recently reported that failed to demonstrate an interaction with LcrV using a yeast two-hybrid system. This variant was able to block secretion of LcrV and Yops, further supporting the hypothesis that the formation of an LcrV-LcrG complex is required for Yop secretion (19).

In this context, elucidation of details of molecular interactions involved in LcrV complex formation is fundamental to understanding secretion processes in *Yersinia* pathogenesis. However, a lack of any quantitative protein interaction information has motivated us to produce pure folded recombinant forms of these proteins. Using these materials, we report the relative affinities of LcrV for itself and for LcrG. In addition, the availability of such materials has afforded us the opportunity to produce site-directed mutants of LcrV within the predicted coiled-coil motif and subsequently assess the importance of this motif both in terms of LcrG interaction and Yop secretion. Therefore, the present investigation provides the first quantitative characterization of type III secretion protein-protein interactions and a more detailed molecular description of LcrV and LcrG folding and complex formation, which complements previous genetic approaches.

EXPERIMENTAL PROCEDURES

Materials—Oligonucleotides were purchased from Sigma. Media reagents Luria Broth (LB) and Brain-Heart infusion were obtained from Merck. Isopropyl-1-thio- β -D-galactopyranoside was from Genesys (London, UK). Precast native and SDS-polyacrylamide gels, protein molecular weight standards, Coomassie Brilliant Blue, glutathione-Sepharose 4B, Hybond-P nitrocellulose membrane, ECL detection reagents, and Factor Xa were from Amersham Biosciences. 30% polyacrylamide solution for 14% PAGE was purchased from Severn Biotech (Kidderminster, United Kingdom). DNA QiaQuick gel extraction and Miniprep kits were from Qiagen. Restriction enzymes were purchased from New England Biolabs Ltd. (Hitchin, United Kingdom). PCR reagents including *Pfu* polymerase were obtained from Stratagene. Protein Centriprep-concentrating devices were purchased from Millipore (Bedford, MA). Bradford assay reagent and disposable plastic columns were obtained from Bio-Rad. Kodak X-Omat AR was purchased from Eastman Kodak Co. Dextran-coated CM5 sensor chips and detergent P20 were purchased from BIAcore (Uppsala, Sweden). Suprasil cuvettes were from Helma Kuvetten (Mulheim, Germany). All antibodies for enzyme-linked immunosorbent assay (ELISA) and Western blotting, apart from mouse anti-LcrV (Defence Science and Technology Laboratory, Wiltshire, United Kingdom), were purchased from Sigma. Marvel dried skimmed milk powder used as a source of casein was from Premier Beverages (Stafford, United Kingdom). All other chemicals were purchased from Sigma.

Construction of Plasmids and Site-directed Mutants—Plasmids pGEX-V and pGEX-G are pGEX-5X1 derivatives (Amersham Biosciences). Both plasmids encode *Schistosoma japonicum* glutathione S-transferase (GST), a linker peptide containing a protease cleavage site, and either the *Y. pestis* LcrV (pGEX-V) or LcrG (pGEX-G) proteins. The genes encoding *lcrV* and *lcrG* were ligated into the *EcoRI*-*NotI* sites of the pGEX-5X-1 vector. pGEX-V was generated by a *Pfu*-based PCR of *lcrV* using Primer1 (5'-ATCGAATTCATTAGAGCCTACGAACAAAAC-3'), which contains an *EcoRI* restriction site upstream of the second

codon (ATT), and Primer2 (5'-ACATAGTATAGCGGCCGCGTGCATT-TACCAGACGT-3'), which incorporates a unique *NotI* site downstream of the TCA stop codon. pGEX-G was generated by a *Pfu*-based PCR of *lcrG* using Primer3 (5'-ATAGAATTCACAAATAATATCAAGACAGACAGC-3'), which contains an *EcoRI* restriction site upstream of the second codon (ACA), and Primer4 (5'-ACATAGTATAGCGGCCGCGCAT-ATTAAATAATTTGCCCTCGCAT-3'), which contains a *NotI* restriction site downstream of the TAA stop codon. pGEX-V and pGEX-G were subsequently transformed into the *E. coli* strain BL21 (DE3) for overproduction of recombinant GST-LcrV or GST-LcrG fusion proteins, respectively. Plasmid pGEX-V was purified using the Qiagen QiaQuick Spin Miniprep kit and then used as a template to amplify the *Y. pestis lcrV* gene in a *Pfu*-based PCR. Primer1 was used with Primer5 (5'-CCCAAGCTTGTGCATTTACCAGACGT-3'), which incorporates a unique *HindIII* site downstream of the TGA stop codon. The 990-bp *lcrV* fragment was ligated into the *EcoRI* and *HindIII* sites of the pTrc99A expression vector (Amersham Biosciences) to produce plasmid pTrc-LcrV. Initial clones were obtained by heat-shock transformation (21) into *E. coli* strain BL21 (DE3).

PCR-based mutagenesis of *lcrV* was performed using the primer overlap method. In all cases, Primer1 was used in conjunction with a "mutagenic" primer containing a site-directed mutation to generate a PCR fragment encoding from the 5' end of the gene to a few bases downstream of the mutation site. A second PCR fragment was generated from a few bases upstream of the mutation site using an overlapping primer, complementary around the mutation site, in combination with Primer2. Each PCR was carried out using pGEX-V as the template. Fragments generated were gel-purified and subjected to a second round of PCR using Primer1 and Primer2 to generate a fragment containing the entire *lcrV* gene with the mutations of choice. Each fragment was then ligated into the *EcoRI* and *NotI* sites of the GST fusion vector pGEX-5X-1 and transformed (21) into *E. coli* strain BL21 (DE3). The resulting plasmids were then used as templates for PCR using Primer1 and Primer5 as described above. The resulting PCR fragments were subsequently ligated into the *EcoRI* and *HindIII* sites of the pTrc99A expression vector. All mutants constructed in the *lcrV* gene contained the CGT codon encoding an arginine residue at positions within the DNA sequence predicted to encode the coiled-coil motif of interest. The presence of desired mutations within the *lcrV* gene was confirmed by sequencing the pGEX-5X-1-*lcrV* plasmids with an automated Applied Biosystems 377 DNA Sequencer (Foster City, CA) using the dideoxy method with BigDye Terminator Ready Reaction Kits (Applied Biosystems, Foster City, CA).

Identification of the putative coiled-coil motifs in LcrV and LcrG was made using the COILS program (ulrec3.unil.ch/coils/COILS_doc.html) (22, 23). A 28-residue window size was used with weighting in favor of hydrophobic residues at the *a* and *d* positions of the heptad repeat. The MATCHER program (cis.poly.edu/~jps/) (24) was also used to determine whether a protein sequence contains the 7-residue periodicity ($[aXX-dXXX]_n$) associated with coiled-coils. Secondary structure predictions were conducted using PHDsec from EMBL (www.embl-heidelberg.de/Services/index.html).

Protein Purification—GST, GST-LcrG, GST-LcrV, and GST-LcrV mutant proteins were purified with minor modifications to a previously described protocol (20). Two liters of LB containing 100 μ g/ml ampicillin were inoculated with 50 ml of an overnight culture of *E. coli* BL21 (DE3) transformed with the appropriate pGEX derivative. Cells were grown at 37 °C with shaking for 2 h and then induced with isopropyl-1-thio- β -D-galactopyranoside to a final concentration of 1 mM. Growth was allowed to continue for another 4 h. Centrifugation of the culture yielded a cell pellet that was resuspended in phosphate-buffered saline (PBS) (0.01 M phosphate buffer, 0.0027 M KCl, 0.137 M NaCl, pH 7.4). Cells were lysed by sonication, and insoluble material was removed by centrifugation at 12,000 $\times g$ for 45 min.

6 ml of 50% (w/v) glutathione-Sepharose 4B in PBS were added to the cell lysate supernatant (typically 12 ml) and incubated at 4 °C for 1 h with rotation. The material was transferred into a plastic column and washed with 100 ml of PBS. GST and GST-LcrV proteins were eluted after this stage by resuspending the glutathione-Sepharose in 6 ml of 10 mM glutathione in 100 mM Tris HCl, pH 8.0, and collecting the flow-through from the column. Otherwise, the glutathione-Sepharose with bound fusion proteins was resuspended in 6 ml of PBS. Proteolytic cleavage to release LcrV or LcrG was conducted by adding 200 μ l of 100 μ g/ml Factor Xa in PBS followed by incubation at 4 °C for 16 h with rotation. Cleaved protein was collected as flow-through from the column. The column was then washed to retrieve all of the protein released. Proteins produced from Factor Xa cleavage all contained five N-terminal residues (GIPEF) prior to the second encoded residue of the predicted protein sequence.

Pooled samples of LcrV were concentrated in Centrprep-YM10 concentrators, whereas pooled LcrG samples required Centrprep-YM3 concentrators. Protein concentrations were determined by Bradford assay. Protein purity was estimated by 8–25% SDS-PAGE, and for LcrV and LcrG by MALDI-MS at the Mass Spectrometry Facility, Department of Biochemistry, University of Bristol (Bristol, United Kingdom).

Circular Dichroism Spectra—Circular dichroism (CD) measurements were performed on an AVIV 62DS spectropolarimeter. The instrument was calibrated with camphor sulfonic acid for optical rotation and benzene vapor for wavelength. Data were recorded at 0.2-nm intervals and at 25 °C in a temperature-controlled chamber. Samples of LcrV wild type and mutants (4 mg/ml in PBS), LcrG (9 mg/ml in PBS), GST (6 mg/ml in PBS), GST-LcrV (4 mg/ml in PBS), or base lines consisting of PBS were examined in 0.001-cm path length Suprasil cuvettes. A minimum of five scans was collected for every sample. Individual scans were smoothed with a Savitsky-Golay filter (25), and the averaged base-line spectrum was subtracted from the averaged sample spectrum. Mean residue molecular weights of 114.2 for LcrV, 110.2 for LcrG, 116.7 for GST, and 115.1 for GST-LcrV were used in the calculations of mean residue ellipticity.

Spectra were analyzed using the Dichroweb server (26). Reference data sets 4 and 7 (27, 28), which were compatible with the wavelength range obtainable in this study, were used. To test the reliability of the determinations, a number of alternative algorithms were used for the structure calculations: SELCON3 (29, 30), CONTIN (31, 32), and CDSSTR (27). As a means of comparison of the goodness-of-fit of the various methods, the NRMSD parameter (34) was calculated. NRMSD is defined as: $\sum[(\theta_{\text{exp}} - \theta_{\text{cal}})^2 / (\theta_{\text{exp}})^2]^{1/2}$ summed over all wavelengths, where θ_{exp} and θ_{cal} are, respectively, the experimental ellipticities, and the ellipticities of the back-calculated spectra for the derived structure. NRMSD values of <0.1 mean that the back-calculated and experimental spectra are in close agreement (35). A low NRMSD is not sufficient to indicate a correct analysis, but a poor (high) NRMSD generally means the analysis is not correct. In this study, all values were well below 0.1. Calculations of standard deviations between measurements were performed at all wavelengths to determine the variation within a data set.

Gel Electrophoresis and Staining—Purified protein samples were analyzed using 8–25% polyacrylamide gradient Phast gels on a Phast electrophoresis system (Amersham Biosciences). SDS and native gels were stained with Coomassie Brilliant Blue using the Phast system developer unit. Protein interaction studies involved the co-incubation of LcrG with LcrV or GST-LcrV at an estimated 2:1 molar ratio at 4 °C for 30 min prior to visualization on a native 8–25% gel. Identification of protein secretion patterns from *Y. pseudotuberculosis* was done using 14% homogeneous polyacrylamide gels using a Novex Mini-gel system (Novex, San Diego, CA). 25 μ l of 5 \times concentrated protein loading buffer (62.5 mM Tris-HCl, pH 6.8, 2% SDS (w/v), 5% β -mercaptoethanol (v/v)) were used to resuspend protein samples, which were then boiled for 10 min. 10- μ l samples were electrophoresed on gels in a Tris-glycine buffer (21).

Western Blotting—Proteins were separated on an 8–25% gradient Phast gel and transferred onto a nitrocellulose Hybond-P membrane, which was blocked overnight at 4 °C with 5% casein in PBST (PBS containing 0.05% Tween 20 (v/v)). LcrV was detected using a mouse-generated anti-LcrV antibody diluted 1:3000 in PBST + 5% casein and incubated for 1 h at room temperature. After washing, membranes were incubated with an anti-mouse horseradish peroxidase-conjugated antibody (1:10,000 in PBST) for 1 h at room temperature. Horseradish peroxidase was detected using ECL reagents and visualized by exposure of Kodak X-Omat AR film.

Binding Assays—ELISA methods were used to analyze interactions between GST-LcrV and LcrV (self-association), GST-LcrV and LcrG, and LcrV and LcrG based upon related studies of the enteropathogenic *E. coli* EspA protein (36). The self-association of LcrV was assayed by incubating 100 μ l of aliquots of LcrV at 20 μ g/ml in carbonate/bicarbonate buffer (0.05 M carbonate/bicarbonate buffer, pH 9.6) in an ELISA plate at 4 °C overnight. Wells were washed three times with 200 μ l of PBST and blocked with 200 μ l of 2% (w/v) casein in PBST for 1 h at 37 °C. 70 μ l of GST-LcrV at concentrations ranging from 0.2 to 2 mg/ml in PBST containing 1% casein (w/v) were added to wells and incubated at 37 °C for 1.5 h. After washing, 70 μ l of rabbit anti-GST IgG (1:5000 dilution in PBST) were added to each well for 1 h at 37 °C. Further washing was followed by 70 μ l of alkaline phosphatase-conjugated anti-rabbit antibody (1:5000 dilution in PBST) being added to wells and incubated for 1 h at 37 °C. The reaction was visualized by adding 70 μ l of 1 mg/ml ρ -nitrophenylphosphate in 100 mM Tris-HCl, pH 9.5, and

observing the optical density measured at 405 nm after 20 min. The mean optical density and mean \pm S.D. were calculated from triplicate experiments, and the K_D was estimated using a GST-LcrV molecular mass of 64,000 and a single-site ligand binding model (Grafit v3.09, Erithacus Software Ltd., United Kingdom). The interaction of GST with immobilized LcrV was measured as a control for nonspecific binding. The association of GST-LcrV with LcrG was assayed as just described with the exception that LcrG was immobilized at 20 μ g/ml to the ELISA plate and that subsequent incubation with GST-LcrV was performed at concentrations ranging from 0.19 to 100 μ g/ml. The interaction of GST with immobilized LcrG was measured as a control for nonspecific binding.

The LcrV-LcrG interaction was assayed by coating an ELISA plate with 100 μ l of 20 μ g/ml LcrG as described above. After washing, wells were blocked with 1% bovine serum albumin (w/v) in PBST. 100 μ l of LcrV at concentrations between 0.07 and 80 μ g/ml in PBST were added to the wells for 2 h at 37 °C. Plates were washed and probed with a mouse anti-LcrV monoclonal antibody (1:2000 dilution in PBST at 37 °C for 1 h) followed by alkaline phosphatase-conjugated anti-mouse antibody (1:2000 dilution, 37 °C for 1 h). The reaction was visualized, and the K_D was estimated using an LcrV molecular mass of 37,000 as described above. LcrV binding to the ELISA plate was used as a control.

The affinity of LcrV for LcrG was determined using surface plasmon resonance (SPR) (37) in a BIAcore X instrument with dextran-coated CM5 sensor chips. LcrG at 15 μ g/ml in a sodium acetate/acetic acid buffer, pH 6.0, was immobilized to a CM5 chip by amine coupling (38). The injection of 100 μ l of 0.1–1.2 μ M wild type and mutant LcrVs in HEPES-buffered saline (10 mM HEPES, 150 mM NaCl, 0.01% (w/v) detergent P20) was performed at a flow rate of 20 μ l/min. The binding surface was regenerated with 30 μ l of 10 mM HCl at 20 μ l/min, which restored the base-line response level without degradation of the sensor chip. The binding of LcrV at all concentrations to the CM5 dextran chip alone was subtracted from the experimental data as a control.

In addition, LcrV at 15 μ g/ml in a sodium acetate/acetic acid buffer, pH 6.0, was immobilized to a CM5 chip by amine coupling (38). The injection of 100 μ l of 0.7–8.0 μ M wild-type LcrG in HEPES-buffered saline was performed at a flow rate of 20 μ l/min. The binding surface was regenerated with 30 μ l of 10 mM HCl at 20 μ l/min. The binding of LcrG at all concentrations to the CM5 dextran chip alone was subtracted from the experimental data as a control.

Sensorgrams were analyzed using the BIAevaluation 3.0 package (BIAcore, Uppsala Sweden) to derive values for association rate constants (k_a) and dissociation rate constants (k_d) by simultaneously fitting several data sets, consisting of injections over a range of ligand concentrations using simple 1:1 Langmuir binding models with the global fitting option. The K_D value was derived from k_d/k_a . A second estimate of the K_D was derived from a plot of the response levels at equilibrium against protein concentration. A steady-state affinity model was used to fit the curve.

Protein Secretion Assays—Analyses of secretion patterns of Yops in *Y. pseudotuberculosis* were conducted according to a previously described method (10). For production of competent cells, *Y. pseudotuberculosis* strain YPIII containing the pIB19 variant of the *Yersinia* pYV plasmid (*lcrV* Δ amino acids 10–313) (10) was grown in LB at 37 °C overnight with 30 μ g/ml kanamycin. Dilution 1:150 into 200 ml of LB with 30 μ g/ml kanamycin was followed by growth at 37 °C to $A_{600} = 0.6$. Cells were harvested, resuspended in 500 ml of distilled H₂O, centrifuged, resuspended in 5 ml of 10% glycerol, centrifuged again, and finally resuspended in 400 μ l of 10% glycerol. Plasmids pTrc99A, pTrc-LcrV, and pTrc99A derivatives containing *lcrV* coiled-coil mutants were transformed into competent *Y. pseudotuberculosis* strain YPIII (pIB19) by electroporation. For Yop induction assays, single colonies of *Y. pseudotuberculosis* YPIII (pIB19) and the same strain transformed with pTrc99A and its derivatives were each inoculated into 5 ml of calcium-depleted Brain-Heart infusion medium (BHI) including 5 mM EGTA, 20 mM MgCl₂, and 0.1% Triton X-100 containing 30 μ g/ml kanamycin and 100 μ g/ml ampicillin and grown overnight at 26 °C. A 1:20 dilution into 10 ml of BHI was grown for 1 h at 26 °C and then for 3 h at 37 °C. Cells were harvested, and the supernatant passed through a 0.45- μ m filter (Millipore). Supernatants were precipitated with 10% trichloroacetic acid as described previously (39). The volumes of 5 \times SDS sample buffer used to resuspend the protein samples (typically \sim 25 μ l) were calculated to normalize for small variations in the final observed A_{600} values measured from the original bacterial cultures. Proteins were separated by 14% SDS-PAGE and visualized by Coomassie Brilliant Blue staining.

RESULTS

Identification of Coiled-coiled Motifs—Protein sequences along with secondary structure and coiled-coil motif predictions are shown in Fig. 1 for regions of LcrV and LcrG with the highest probabilities of containing a helix capable of forming a coiled-coil. For LcrV, the COILS program (ulrec3.unil.ch/coils/COILS_doc.html) gave a probability of 0.988 that the helical sequence (PHDsec) will adopt a coiled-coil conformation, whereas the MATCHER program and helical wheel plot (marqusee9.berkeley.edu/kael/helical.htm) identified residues Leu-153, Leu-157, Leu-160, and Leu-164 as being central within this region and present in crucial *a* and *d* heptad repeat positions. The probability of the α -helix in LcrG (PHDsec) forming coiled-coil interactions was 0.806. Residues Leu-13, Ala-16, and Ile-20 were identified as being central within the region

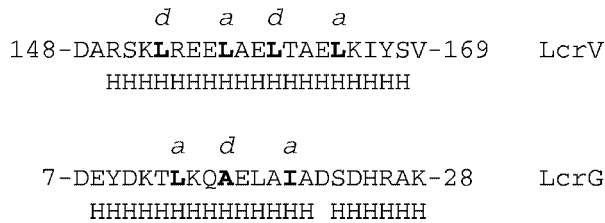


FIG. 1. **Prediction of coiled-coil regions in both LcrV and LcrG.** The COILS program was used with a 28-residue window size and a weighting of 2.5 toward the presence of hydrophobic residues (*boldface*) at positions *a* and *d*. The MATCHER program confirmed regions with 7-residue periodicity (indicated by *a* and *d*), whereas the prediction of a helical structure was carried out using PHDsec.

and at positions indicative of the presence of a coiled-coil motif in this protein.

Protein Production and Folding—GST and GST-LcrV, purified following elution from the glutathione-Sepharose 4B column, migrated as single bands of ~27 and 64 kDa, respectively, using SDS-reducing PAGE. LcrV and LcrG purified following Factor Xa cleavage from the GST fusion tag also migrated as single bands at 37 and 11 kDa, respectively. Using MALDI-MS, LcrV had a molecular mass of 37,720 Da compared with 37,652 Da by calculation, whereas LcrG had a molecular mass of 11,491 Da compared with 11,432 Da by calculation. Prior to purification of the LcrV mutants, the presence of the desired mutations in the pGEX-5X-1-*lcrV* plasmids used for expression was confirmed. In all cases, the desired sequence was observed (compared with the published entry in GenBank™ (www.ncbi.nlm.nih.gov/)) with the required changes that are always present as a CGT codon encoding an arginine residue. Subsequent purification of LcrV mutants using the glutathione-Sepharose 4B column yielded proteins with the same apparent molecular mass and purity (judged by SDS-PAGE) as that observed for the wild-type protein.

The CD spectra of LcrG and LcrV cleaved from the GST moiety (Fig. 2A) exhibit similar features, namely a maximum at 192 nm and minima at 208 and 222 nm that are characteristic of proteins with a significant α -helical content but with other secondary structures present. The results reported in Table I are for the CDSSTR secondary structure method (27) with reference data base 4 (26), which gave the best fits (lowest NRMSDs). However, in general, all calculations produced very

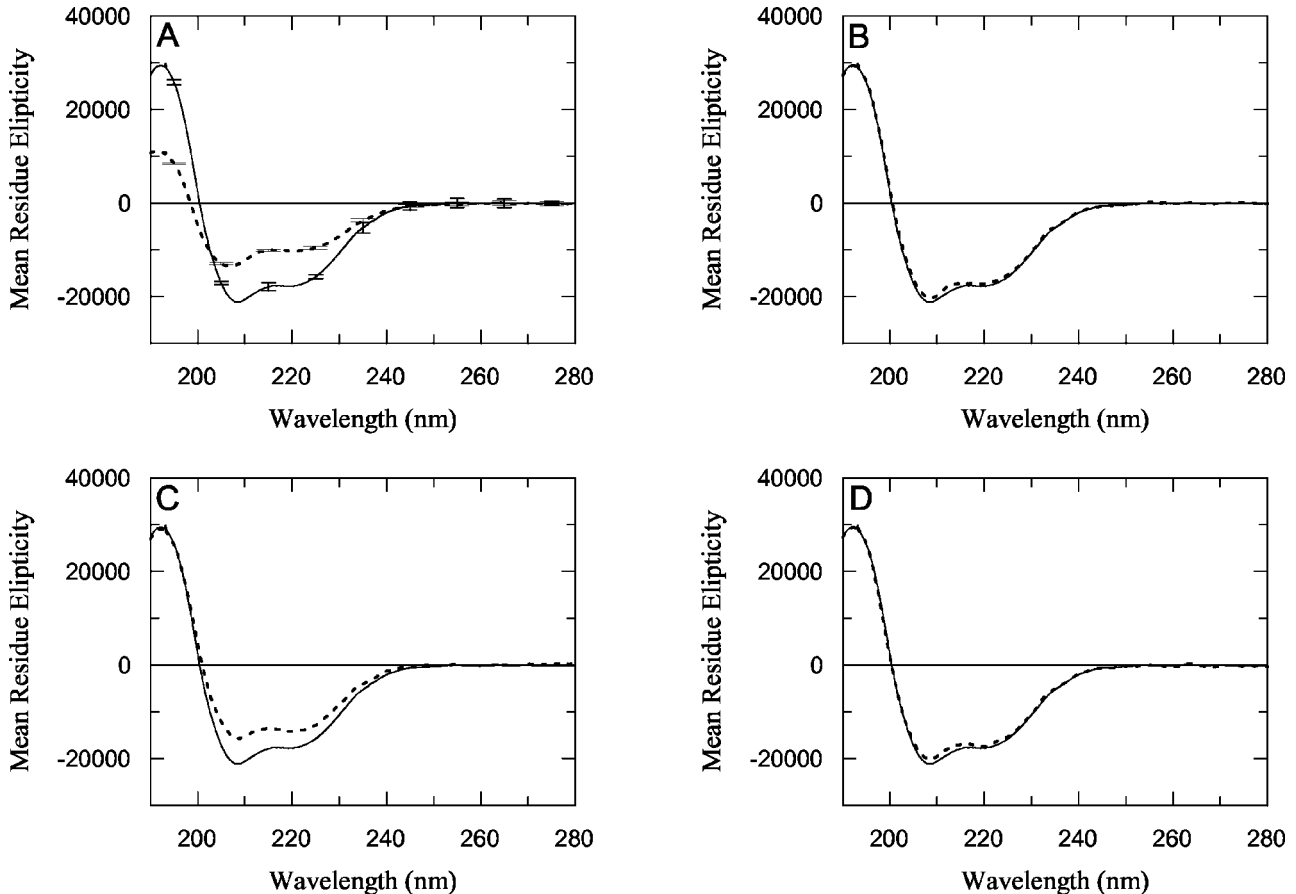


FIG. 2. **CD spectra for wild-type LcrV, LcrG, and LcrV mutant proteins cleaved from their GST- moieties.** Data are represented as mean residue ellipticity and were recorded at 4 mg/ml (LcrV, *solid line*) and 9 mg/ml (LcrG, *dashed line*) at 0.2-nm scan steps (*panel A*). The *error bars* in the data for repeated scans are represented only in *panel A* for clarity but are representative of all data collected. *Panels B–D* show a comparison of the spectra between LcrV wild-type (*solid line*) and mutant (*dashed line*) proteins (L157R, L153R, and L153R/L164R, respectively), which were obtained using 4 mg/ml of each protein.

TABLE I
Secondary structure analysis from CD data

Protein	% Secondary structure				Total	NRMSD
	α helix	β -strand	β turn	Other		
LcrV wild type	58 \pm 1.1	8 \pm 1.9	13 \pm 1.3	22 \pm 3.3	101	0.010
LcrV L153R	49 \pm 1.3	11 \pm 2.7	15 \pm 1.1	25 \pm 1.9	100	0.009
LcrV L157R	56	7	13	24	100	0.011
LcrV L160R	50	13	14	23	100	0.011
LcrV L164R	58	7	13	22	100	0.012
LcrV L153/157R	51	9	15	24	99	0.013
LcrV L153/160R	53	9	13	25	100	0.009
LcrV L153/164R	59	7	12	23	101	0.012
LcrV L157/160R	49	12	14	24	99	0.014
LcrV L157/164R	52	9	14	25	100	0.010
LcrV L160/164R	53	8	14	25	100	0.014
LcrG wild type	35 \pm 1.4	16 \pm 1.3	21 \pm 1.9	29 \pm 1.0	101	0.014

similar secondary structures. For wild-type LcrV, the calculated secondary structure is 58% helix, 8% β -sheet, 13% turn, and 22% other compared with 56% helix, 8% β -sheet, and 36% loop proposed by secondary structure predictions (PHDsec). For wild-type LcrG, the calculated secondary structure is 35% helix, 16% β -sheet, 21% turn, and 29% other compared with 60% helix, 0% β -sheet, and 40% loop proposed by secondary structure predictions (PHDsec). The CD spectra of GST and GST-LcrV also exhibited features demonstrating significant α -helical content (data not shown). The former spectrum is consistent with the known crystal structure of GST (40). The absence of significant changes in non-helical features in the GST-LcrV spectrum suggests that there is no gross disruption in the conformation of either protein.

The LcrV mutants displayed a range of spectral features. Many of these proteins produce spectra that are indistinguishable from wild-type LcrV (e.g. L157R, Fig. 2B), and consequently, their calculated secondary structures are identical (Table I). However, other mutants produced slightly different spectra (e.g. L153R, Fig. 2C), which in some cases could appear similar to a wild-type spectrum upon the addition of a second mutation (e.g. L153R/L157R, Fig. 2D). When compared with wild-type LcrV, all mutants had an equivalent 192-nm peak, but the magnitudes and ratios of the 208- and 222-nm peaks were altered in some cases (Table II). Consequently, the calculated α -helical content of these mutants tended to be lower than that of the wild-type protein (Table I). These data provide evidence for alterations in the secondary structure and perhaps the tertiary structure (coiled-coil) interactions of the mutants. However, it should be noted that none of the mutant structures was radically altered in the sense of producing unfolded proteins as a consequence of the replacement of leucine with arginine residues in the predicted coiled-coil motif.

Native Gel Electrophoresis—When analyzed by native PAGE, purified LcrV appears to migrate as a mixture of forms (Fig. 3, lane 1). The lowest migrating band is the predominant species, which corresponds to the formation of a dimer with an estimated molecular mass of 74 kDa. Higher migrating bands, which can appear as doublets, represent higher order oligomers that may adopt subtly different conformations depending upon the mode of association perhaps arising from coiled-coil and other inter-domain interactions. No LcrV monomer was visible on the native gel, and no evidence of degradation was observable using SDS-reducing PAGE as reported earlier. Native PAGE of the GST-LcrV fusion also showed a mixture of forms, upshifted in comparison to Fig. 3 arising from the presence of GST (data not shown). In contrast, LcrG appears as a single species on the native gel (Fig. 3, lane 2) with an estimated molecular mass corresponding to an 11-kDa monomer. The addition of a 2:1 molar excess of LcrG to LcrV (Fig. 3, lane 3) results in a distinct downshift of the 74-kDa dimer band of

LcrV, suggesting the formation of a heterodimer between LcrV and LcrG. The effects of the Leu to Arg substitutions upon the ability of LcrV to multimerize were also analyzed by native PAGE analysis. Variable mobility was observed between the different LcrV mutants. In general, both single and double mutations appear to reduce the level of multimerization of the protein with double substitutions doing so to a greater extent (Table II).

Protein-Protein Interactions—ELISA assays were carried out to assess the binding of LcrV to LcrG and the interaction of LcrV with itself. Fig. 4A shows the results obtained using LcrG-coated microtiter wells, which were probed with LcrV. Fitting to a single-site isotherm gave a good estimate for the K_D of 208 \pm 20 nM. Using GST-LcrV instead of LcrV, a similar dissociation constant was obtained ($K_D = 150 \pm 12$ nM). No appreciable nonspecific binding to LcrG was observed using GST alone. This suggests that the interaction observed with the GST-LcrV fusion is between the LcrV domain and LcrG and is of a similar nature to that observed using purified LcrV isolated after Factor Xa removal of GST. Fig. 4B shows the ELISA results obtained for the binding of GST-LcrV to LcrV-coated microtiter wells. Fitting to a single-site isotherm gave $K_D = 1.13 \pm 0.11$ μ M. Low nonspecific binding was observed using GST alone, suggesting that the interaction is specific for LcrV. Fig. 5 shows overlaid sensorgrams of LcrV binding to LcrG immobilized to the CM5 dextran chip and then fitting of the data using a simple 1:1 Langmuir binding model. This yielded $K_D = 140$ nM ($\chi^2 = 1.15$; $k_a = 4.38^{+3}$ 1/ms, $k_d = 5.41^{-4}$ 1/s), similar to that obtained using ELISA methods. The reliability of the data was reinforced by plotting the response unit values at equilibrium against ligand concentration, which generated a binding curve reaching saturation at higher concentrations. A fit to this data gave an estimated $K_D = 135$ nM ($\chi^2 = 0.0435$). Inverting the system by immobilizing LcrV to the CM5 dextran chip to follow LcrG binding was also attempted. Although the small size of LcrG (11 kDa) meant that the observed relative unit levels were only measurable at high concentrations of LcrG, an estimated $K_D = 544$ nM ($\chi^2 = 0.154$) was obtained. This value is comparable with those obtained from ELISA assays and SPR methods as already described.

In most cases, the mutations of Leu to Arg in the predicted coiled-coil motif of LcrV reduced binding to LcrG. ELISA assays (Fig. 4, C and D) yielded K_D values ranging from \sim 400 nM to 2.2 μ M (summarized in Table II), and insignificant levels of binding (<15 response units) were observed using SPR. The exceptions are two mutants, L153R and L157R/L160R, which bound to LcrG with dissociation constants similar to that of the wild-type LcrV measured using both ELISA and SPR methods (Fig. 4E and Table II).

Secretion Profiles—SDS-PAGE of culture filtrates of *Y. pseudotuberculosis* strain YPIII pIB19 (lacking the *lcrV* gene)

TABLE II
A summary of information obtained for LcrV wild type and mutant proteins

LcrV	Wild-type	L153R	L157R	L160R	L164R	L153R/L157R	L153R/L160R	L153R/L164R	L157R/L160R	L157R/L164R	L160R/L164R
CD ratio of 208 nm peak to wild type	1.0	0.745	0.963	0.667	0.978	0.757	0.859	0.953	0.682	0.811	0.829
CD ratio of 208 nm to 222 nm peaks	1.189	1.112	1.176	1.088	1.158	1.110	1.155	1.157	1.049	1.118	1.115
Multimerisation											
K_D (nM) for LcrG by ELISA	208	16.0	693	605	697	2180	118	4400	589	432	641
K_D (nM) for LcrG by SPR	140	235	n.d. ^a	n.d. ^a	n.d. ^a	n.d. ^a	278	n.d. ^a	n.d. ^a	n.d. ^a	n.d. ^a
Secretion pattern from <i>Yersinia pseudotuberculosis</i>											

^a n.d., not determined. Interaction of LcrV mutant with LcrG chip generated <15 RU.

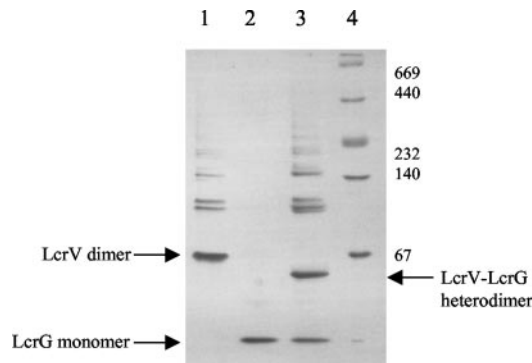


FIG. 3. **Native gel analysis of LcrV and LcrG.** LcrV migrates as a mixture of dimeric and multimeric species (1). Upon the addition of LcrG (2), a downshift in the LcrV dimer band occurs (3). An estimated 2:1 molar ratio of LcrG was added to 4 mg/ml LcrV, incubated at 4 °C for 30 min, and run on an 8–25% native PAGE gel using the Phast system. Native molecular weight markers (4) used were thyroglobulin (669,000), ferritin (440,000), catalase (232,000), lactate dehydrogenase (140,000), and albumin (66,000).

or the same strain transformed with plasmid pTrc99A did not show significant levels of secreted Yops as expected. Transformation with pTrc-LcrV (containing the wild-type *lcrV* gene) restored Yop release, whereas the pTrc99A derivatives containing *lcrV* coiled-coil mutants generated a range of secretion patterns (Table II). Western blotting confirmed equal levels of expression of LcrV from the pTrc-LcrV wild-type and mutant constructs in each transformant (data not shown).

The secretion patterns can be roughly grouped into two sets. The first set demonstrated greatly reduced levels of Yop secretion compared with *Y. pseudotuberculosis* complemented with wild-type LcrV. This includes clones that were mutated in either of the two central leucine residues (L157R or L160R) and double mutants that include at least one of these leucines (L157R/L160R, L157R/L164R, or L160R/L164R). The second set demonstrated a secretion pattern that was only slightly reduced compared with wild-type LcrV. This includes clones that were mutated at either of the peripheral leucine residues (L153R or L164R) and any double mutant that contained the L153R mutation (L153R/L157R, L153R/L160R, or L153R/L164R).

DISCUSSION

Quantitative Analysis of LcrV Interactions—This paper describes the high level production of LcrV and LcrG wild-type proteins and LcrV mutants, which have been used to establish a quantitative characterization of the protein-protein interactions of LcrV with itself and with LcrG. The virulence of *Y. pestis* has been shown to be related to the presence of the LcrV protein, which is required for the secretion of Yop effector proteins (41). The LcrG protein is a negative regulator of secretion, and in the absence of LcrV, LcrG protein blocks Yop secretion by interacting with the type III secretion apparatus within the cytoplasm of the pathogen (18, 41, 42). Subsequent studies demonstrated the formation of an LcrV-LcrG heterodimer identified in *Y. pestis* by chemical cross-linking (17) and identified in *Y. pestis* and *Y. enterocolitica* by co-purification (11, 17). Recent yeast two-hybrid analysis has also dem-

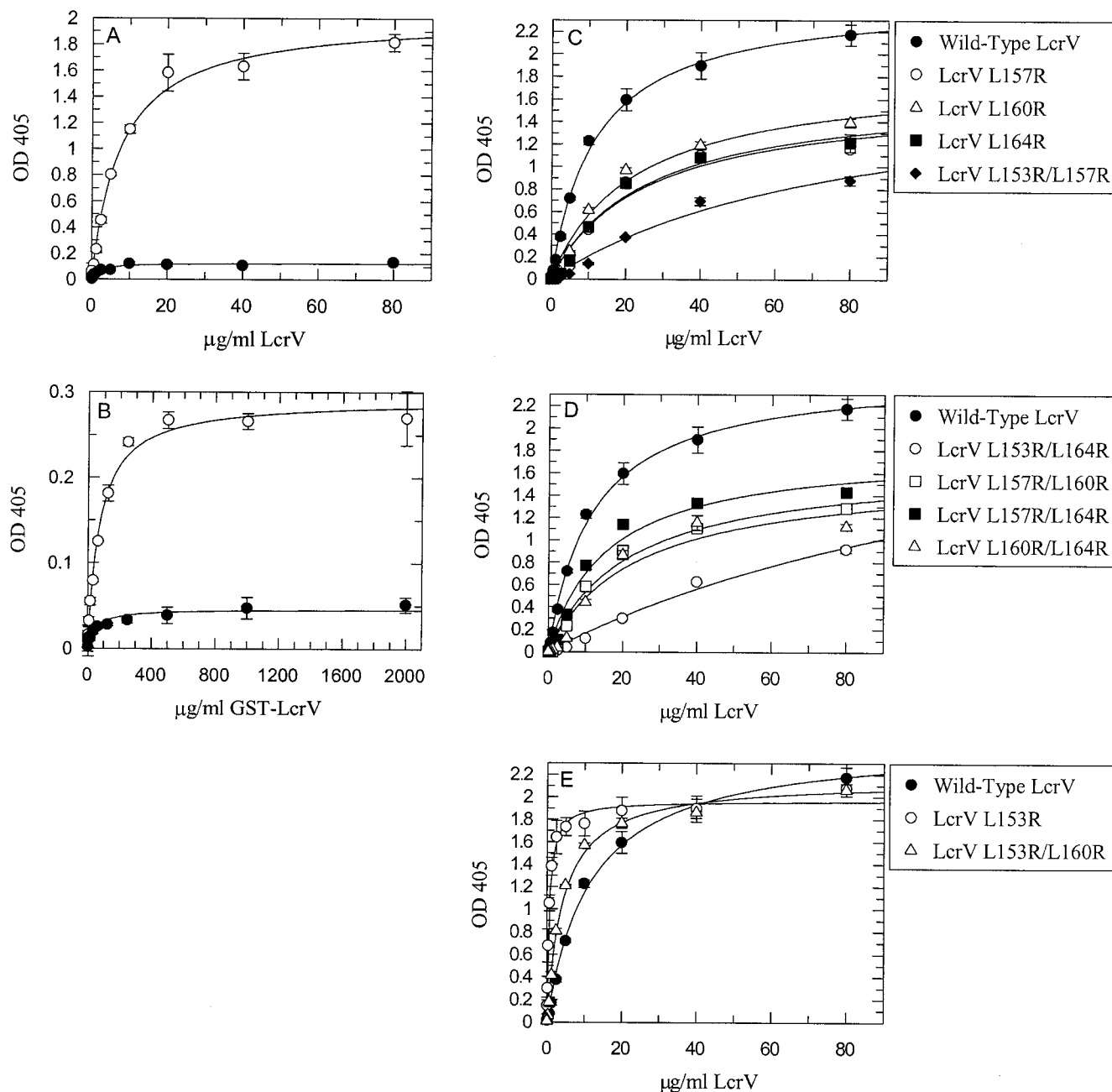


FIG. 4. Binding assays of LcrV interactions. A, the interaction of LcrV with LcrG. LcrG was immobilized to the ELISA plate, and titration with LcrV was shown to bind using mouse anti-LcrV monoclonal antibody and alkaline phosphatase-conjugated anti-mouse antibody (○). The K_d for the interaction was determined as 208 ± 32 nM. The binding of LcrV to the ELISA plate was used as a control (●). B, the interaction of GST-LcrV with LcrV. LcrV was immobilized to the ELISA plate, and titration with Gst-LcrV was shown to bind using anti-GST IgG and alkaline phosphatase-conjugated anti-rabbit antibody (○). The K_d for the interaction was determined as 1.13 ± 0.11 μM . The binding of GST to immobilized LcrV was used as a control (●). C and D, binding of LcrV mutants to immobilized LcrG. These mutants showed lower affinity for LcrG than wild-type LcrV. E, binding of two anomalous LcrV mutants to immobilized LcrG. These mutants have an affinity for LcrG equivalent to or greater than that of wild-type LcrV.

onstrated an interaction between LcrV and LcrG and that this interaction is required for Yop secretion (19).

In these studies, a pure LcrV sample was shown to form multimers of dimers and higher order species as reported recently (43), whereas LcrG appears to be exclusively monomeric in contrast to previous reports (44). This multimerization is dependent upon the concentration of the protein with LcrV existing as a stable dimeric unit at low concentrations (43) in the ELISA and SPR methods. LcrV-LcrG complex formation was first observed using native gel electrophoresis, which yielded a band consistent with heterodimer formation. Subsequently, ELISA and SPR methods demonstrated similar nano-

molar binding affinities between LcrV and LcrG, thus suggesting that complex formation between these two proteins is favored over dimer formation and perhaps over other self-association interactions, the latter of which displays a micromolar binding affinity. The close fit of a 1:1 binding model to the data for LcrV binding to LcrG using SPR indicates that only a single species of LcrV is binding immobilized LcrG. These results support the proposal that *in vivo* LcrV titrates LcrG from the type III secretion apparatus (17) and is in agreement with previous data proposing that the ratio of LcrV to LcrG is important for type III secretion activity (18, 19). Significantly, assuming a stable LcrG-LcrV complex is essential for Yop se-

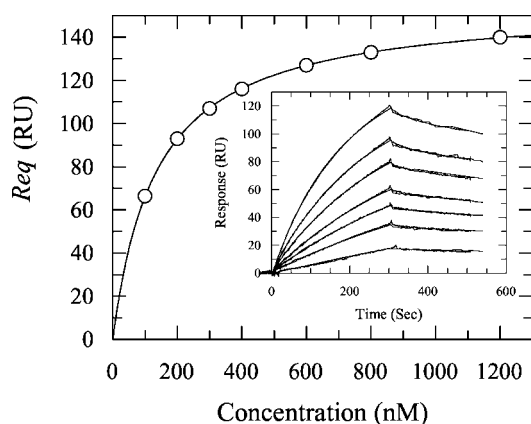


FIG. 5. LcrV binding to LcrG demonstrated by surface plasmon resonance. LcrG was immobilized to a CM5 dextran chip by amine coupling. *Inset*, injection of 0.1–1.2 μM wild-type and mutant LcrVs in HEPES-buffered saline was performed at a flow rate of 20 $\mu\text{l}/\text{min}$, and the binding was measured as response units over time. A simple 1:1 Langmuir binding model was used to fit the data and gave an estimated K_D of $1.40 \times 10^{-7} \text{ M}$ ($\chi^2 = 1.15$). (*main figure*) Data reliability was confirmed by plotting the response unit values at equilibrium (Req) against ligand concentration. A steady-state affinity fit to this data gave an estimated LcrV-LcrG K_D of $1.35 \times 10^{-7} \text{ M}$ ($\chi^2 = 0.0435$).

cretion, the results presented here predict that competing affinities between LcrG and the type III secretion pore complex are less strong than the nanomolar affinity between LcrG and LcrV reported here.

Coiled-coil Interactions—Pallen *et al.* (13) proposed that complex formation in proteins involved in type III secretion could be mediated by the formation of coiled-coil interactions and identified the LcrV-LcrG complex as a possible example based upon the prediction of a coiled-coil motif in both these proteins. The specific residues identified in Fig. 1 as important for coiled-coil formation are located within the regions reported previously (*i.e.* residues 136–180 for LcrV and 7–34 for LcrG) (13). In particular, Leu-153, Leu-157, Leu-160, and Leu-164 of LcrV are located at critical *a* and *d* heptad positions within the center of this region and should interdigitate with the same residues via the formation of a coiled-coil in the LcrV dimer. In the case of LcrG, residues Leu-13, Ala-16, and Ile-20 of LcrG are within the center of this region and are predicted to be important for the same type of interactions in the LcrV-LcrG complex. Analyses of the CD spectra of LcrV and LcrG produced very low values for the NRMSD fit parameter ($\ll 0.1$), which suggest that a reasonable correspondence exists between calculated secondary structure and the experimentally obtained spectra (Table I). Indeed these values for predicted CD calculated structures are very close for LcrV. However, the accuracy of any secondary structure determined is dependent upon the reference databases used in the analyses being constructed from proteins containing the structural features present in the protein under investigation. As none of the existing reference databases include examples of coiled-coiled structures, if LcrV does contain a coiled-coil structure, the analyses may not be completely accurate in absolute terms. It seems probable that a coiled-coil motif could be present in the proteins studied based on one of the characteristics in the spectra: the ratio of the 208-nm peak relative to 222-nm peak. In the spectra of ordinary α -helices, these two peaks are of roughly the same intensity, but this is not true for the LcrV spectra in this study (Table II). It has been suggested that differences in the 208/222 ratio could be the consequence of helix-helix interactions (45–47), so this may provide some support for different extents of coiled-coil being present in these proteins (Table II).

To probe the potential importance of coiled-coil interactions,

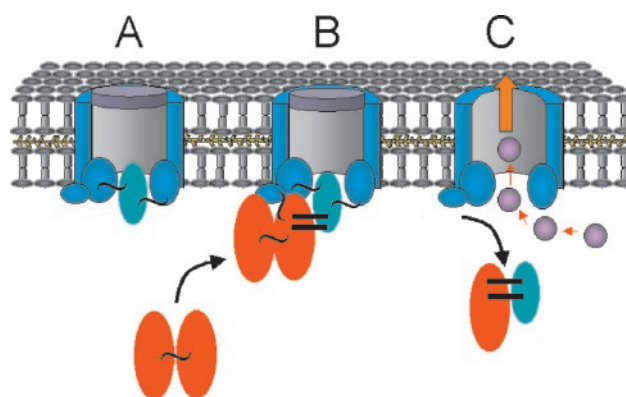


FIG. 6. Interactions inside the Ysc pore of *Yersinia*. A, Yop secretion is repressed by gating of the Ysc apparatus (light blue) externally by LcrE (navy blue), and internally by LcrG (green). It is postulated that LcrG associates with the Ysc components (curved line). B, secretion is induced by the loss of LcrE gating and an increase in the cytoplasmic concentration of LcrV (red). The stable cytoplasmic LcrV dimer dissociates and binds to LcrG with high affinity (solid line). C, secretion is facilitated by the removal of LcrG because of LcrV-LcrG heterodimer formation permitting the release of Yops (purple).

single and all possible double mutants of the leucine residues in LcrV identified in Fig. 1 were made by substituting arginine at these positions. This strategy had previously been shown to be successful in related studies of the EspA and EspD type III secretion pathway proteins from enteropathogenic *E. coli* (36, 16). CD analysis indicated that all LcrV mutants were produced as folded proteins and still showed spectral features, suggestive of helices with possible coiled-coil formation, which may relate to the multimer formation observed in native gels (Table II). At low concentrations in the ELISA and SPR assays, both LcrV wild-type and mutant proteins will be present principally as a dimer. The six single and double mutants of Leu-157, Leu-160, and Leu-164 all showed decreased levels of interaction with LcrG, suggesting that these residues may be involved in coiled-coil interactions with the hydrophobic residues identified in LcrG (Fig. 1). These mutants have reduced on and off rates compared with wild-type LcrV and bind to LcrG in the equilibrium ELISA protocol but not in the flow BIAcore experiments. The mutation of Leu-153 to Arg-, however, resulted in a mutant with a higher affinity for LcrG than the wild-type protein. Although this result does not discount Leu-153 from being involved in a coiled-coil interaction, it is possible that an Arg at this position could mediate other interactions with LcrG. Outside of the heptad repeat region in LcrG, there are numerous aspartate residues (7, 10, 24, 26) that could form a salt-bridge with the mutant Arg-153 side chain of LcrV and result in enhanced affinity between these two proteins. Indeed, using ELISA methods, the interaction of LcrV L153R with LcrG is affected by pH. Furthermore, double mutants involving residue 153 also displayed peculiar behavior. In combination with either the L157R or L164R mutations, double mutants showed the lowest affinity for LcrG, whereas in combination with L160R, wild-type affinity was recovered. These data suggest that the high affinity character of the L153R mutant for LcrG can dominate in some cases depending upon the strength of the disruption caused by the second-site arginine mutation.

Yop Secretion—The current model of the type III secretion apparatus places LcrG on the cytosolic side of the *Yersinia* inner membrane where it forms a plug and blocks the secretion of Yop effector proteins (17). As already discussed, the relatively high affinity between LcrV and LcrG compared with self-interaction of LcrV drives the formation of a heterodimer complex, thus allowing secretion to occur. Based upon this model of interaction, wild-type and the L153R and L153R/

L160R mutants, which all showed high affinity for LcrG, also effectively complemented the *Y. pseudotuberculosis* lcrV knockout and showed predicted high levels of Yop secretion. In addition, single mutants L157R and L160R and double mutants L157R/L160R, L157R/L164R, and L160R/L164R all showed reduced levels of binding to LcrG and, predictably, very low levels of secretion. Therefore, these data suggest that coiled-coil interactions may indeed play a significant role in mediating LcrV-LcrG complex formation.

Interestingly, not all secretion patterns observed follow predictions based upon a titration model involving a discrete interaction between LcrV and LcrG. First, the L164R mutant showed reduced levels of binding to LcrG compared with wild-type LcrV protein, but Yop secretion was only moderately reduced. It is possible that the effects of the Leu-164 mutant were not manifested as greatly as when other residues of the coiled-coil (Leu-157 and Leu-160) were mutated. This is consistent with the almost total loss of secretion when L164R is combined as a double mutant with L157R or L160R (Table II). Although, more curious is the presence of wild-type secretion for the L153R/L157R and L153R/L164R double mutants, both of which display the weakest interactions with LcrG based upon ELISA assays (Table II). One explanation is that *in vivo*, the great increase in intracellular LcrV upon type III secretion stimulation and the high affinity interaction of the L153R mutation dominates, resulting in wild-type activity. However, it is also tempting to speculate that recognition of LcrG by LcrV may not simply involve LcrG alone. In particular, the gating function of LcrG implies that it forms an interaction with the Ysc apparatus located on the cytosolic inner membrane of *Yersinia*. Given the small size of LcrG (11 kDa), it is not unreasonable to consider that LcrV could initially recognize an LcrG-type III secretion apparatus complex prior to the formation of the LcrV-LcrG heterodimer. Although the L153R/L160R and L153R/L164R double mutants show poor interactions with LcrG, it is possible that these proteins may still promote dissociation of LcrG from the type III secretion apparatus, especially if LcrV initially recognizes a complex rather than LcrG on its own.

Taken together, these results lead us to propose a modified model of LcrV-LcrG titration where stable and transient protein complexes are formed and exchanged depending upon relative affinities as a means of regulating type III secretion in *Yersinia*. Under non-secreting conditions, LcrG forms a complex with the Ysc apparatus located on the cytosolic side of the inner membrane (Fig. 6A) (17). Upon induction of type III secretion, high levels of LcrV are produced predominantly as a dimer (Fig. 6B). The high nanomolar affinity of LcrV for LcrG disrupts LcrV dimer formation and interactions between LcrG and the Ysc apparatus. The formation of an LcrV-LcrG complex mediated through coiled-coil interactions as previously proposed (13) results in the removal of the internal gating of the Ysc apparatus, thus enabling Yop secretion to occur (Fig. 6C) (18). In addition, LcrV may initially recognize LcrG as a bound complex near the inner membrane (Fig. 6B) and promote LcrG dissociation through conformational changes, altering the interactions between LcrG and other type III secretion components. The use of the methods developed here to further define the importance of LcrG complex formation and other related pathway components is therefore underway. Furthermore, although the type III secretion system from *Yersinia* is the most studied to date, the system is also present in a number of other pathogenic bacteria such as *P. aeruginosa* where PcrV, a homologue of LcrV, was shown to mediate type III secretion in lung infection (33). Sequence similarities among the different type III components suggest that regulation of Ysc assembly

and secretion may be conserved across species. Hence, it is hoped that characterization of individual protein-protein interactions between pathway components will ultimately yield an improved understanding of the molecular basis of type III secretion processes not only in *Yersinia* but in other bacterial pathogens.

Acknowledgment—We thank Åke Forsberg (the Swedish Defense Research Agency, FOI, Umeå, Sweden) for the kind gift of *Y. pseudotuberculosis* strain YPIII (pIB19).

REFERENCES

- Cornelis, G. R., and Van Gijsegem, F. (2000) *Annu. Rev. Microbiol.* **54**, 735–774
- Hueck, C. J. (1998) *Microbiol. Mol. Biol. Rev.* **62**, 379–433
- Bliska, J. B., Galán, J. E., and Falkow, S. (1993) *Cell* **73**, 903–920
- Miller, J. F., and Cossart, P. (1999) *Curr. Opin. Microbiol.* **2**, 15–17
- Neyt, C., and Cornelis, G. R. (1999) *Society for General Microbiology Symposium, Microbial Signaling And Communication* (England, R. R., Hobbs, G., Bainton, N. J., and Roberts, D. McL., eds) Vol. 57, pp. 215–240, Cambridge University Press, Cambridge, United Kingdom
- Cornelis, G. R. (1998) *J. Bacteriol.* **180**, 5495–5504
- Price, S. B., Cowan, C., Perry, R. D., and Straley, S. C. (1989) *J. Bacteriol.* **171**, 5646–5653
- Burrows, T. W., and Bacon, G. A. (1956) *Br. J. Exp. Pathol.* **37**, 481–493
- Leary, S. E. C., Griffin, K. F., Galyov, E. E., Hewer, J., Williamson, E. D., Holmström, A., Forsberg, Å., and Titball, R. W. (1999) *Microb. Pathog.* **26**, 159–169
- Petersson, J., Holmström, A., Hill, J., Leary, S., Frithz-Lindsten, E., von Euler-Matell, A., Carlsson, E., Titball, R., Forsberg, Å., and Wolf-Watz, H. (1999) *Mol. Microbiol.* **32**, 961–976
- Sarker, M. R., Neyt, C., Stainier, I., and Cornelis, G. R. (1998) *J. Bacteriol.* **180**, 1207–1214
- Fields, K. A., and Straley, S. C. (1999) *Infect. Immun.* **67**, 4801–4813
- Pallen, M. J., Dougan, G., and Frankel, G. (1997) *Mol. Microbiol.* **25**, 423–425
- Burkhard, P., Stetefeld, J., and Strelkov, S. V. (2001) *Trends Cell Biol.* **11**, 82–88
- Lupas, A. (1996) *Trends Biochem. Sci.* **21**, 375–382
- Daniell, S. J., Delahay, R. M., Shaw, R. K., Hartland, E. L., Pallen, M. J., Booy, F., Ebel, F., Knutton, S., and Frankel, G. (2001) *Infect. Immun.* **69**, 4055–4064
- Nilles, M. L., Williams, A. W., Skrzypek, E., and Straley, S. C. (1997) *J. Bacteriol.* **179**, 1307–1316
- Nilles, M. L., Fields, K. A., and Straley, S. C. (1998) *J. Bacteriol.* **180**, 3410–3420
- Matson, J. S., and Nilles, M. L. (2001) *J. Bacteriol.* **183**, 5082–5091
- Leary, S. E. C., Williamson, E. D., Griffin, K. F., Russell, P., Eley, S. M., and Titball, R. W. (1995) *Infect. Immun.* **63**, 2854–2858
- Sambrook, J., Fritsch, E. F., and Maniatis T. (1989) *Molecular Cloning: A Laboratory Manual*, Cold Spring Harbor Laboratory, Cold Spring Harbor, NY
- Lupas, A., Van Dyke, M., and Stock, J. (1991) *Science* **252**, 1162–1164
- Lupas, A. (1997) *Curr. Opin. Struct. Biol.* **7**, 388–393
- Fischetti, G. M., Landau, J. P., Schmidt, P., and Sellers. V. A. (1993) *Information Processing Letters* **45**, 11–18
- Savitzky, A., and Golay, M. J. E. (1964) *Anal. Chem.* **36**, 1627–1639
- Lobley, A., Whitmore, L., and Wallace, B. A. (2002) *Bioinformatics* **18**, 211–212
- Sreerama, N., and Woody, R. W. (2000) *Anal. Biochem.* **282**, 252–260
- Sreerama, N., Vanyaminov, S. Y., and Woody, R. W. (2000) *Anal. Biochem.* **287**, 243–251
- Sreerama, N., and Woody, R. W. (1993) *Anal. Biochem.* **209**, 32–44
- Sreerama, N., Vanyaminov, S. Y., and Woody, R. W. (1993) *Protein Sci.* **8**, 370–380
- Provencher, S. W., and Glockner, J. (1981) *Biochemistry* **20**, 33–37
- Van Stokkum, I. H. M., Spoelder, H. J. W., Bloemendal, M., Van Grondelle, R., and Groen, F. C. A. (1990) *Anal. Biochem.* **191**, 110–118
- Sawa, T., Yahr, T. L., Ohara, M., Kurahashi, K., Gropper, M. A., Wiener-Kronish, J. P., and Frank, D. W. (1999) *Nat. Med.* **5**, 392–398
- Mao, D., Wachter, E., and Wallace, B. A. (1982) *Biochemistry* **21**, 4960–4968
- Brahms, S., and Brahms, J. (1980) *J. Mol. Biol.* **138**, 149–178
- Delahay, R. M., Knutton, S., Shaw, R. K., Hartland, E. L., Pallen, M. J., and Frankel, G. (1999) *J. Biol. Chem.* **274**, 35969–35974
- Markey, F. (1999) *BLA Journal* **1**, 14–16
- BLAcore Ltd. (2001) *BLAtechnology Handbook*, pp. 41–45, Upsala, Sweden
- Forsberg, Å., Bolin, I., Norlander, L., and Wolf-Watz, H. (1987) *Microb. Pathog.* **2**, 123–137
- McTigue, M. A., Williams, D. R., and Tainer, J. A. (1995) *J. Mol. Biol.* **246**, 21–27
- Skrzypek, E., and Straley, S. C. (1995) *J. Bacteriol.* **177**, 2530–2542
- Skrzypek, E., and Straley, S. C. (1993) *J. Bacteriol.* **175**, 3520–3528
- Tito, M. A., Miller, J., Walker, N., Griffin, K. F., Williamson, E. D., Despeyroux-Hill, D., Titball, R. W., and Robinson, C. V. (2001) *Biophys. J.* **81**, 3503–3509
- Boyd, A. P., Sory, M. P., Iriarte, M., and Cornelis, G. R. (1998) *Mol. Microbiol.* **27**, 425–436
- Lau, S. Y. M., Taneja, A. K., and Hodges, R. S. (1984) *J. Biol. Chem.* **259**, 13253–13261
- Zhou, N. E., Zhu, B., Kay, C. M., and Hodges, R. S. (1992) *Biopolymers* **32**, 419–426
- Woolley, G. A., and Wallace, B. A. (1993) *Biochemistry* **32**, 9819–9825